Size-Controllable Synthesis and Characterization of Wide Band Gap Semiconductor Oxide Nanoparticles

A.Sharma*, A. Sharma**, R. Sharma***
*Electrical Engineering Department, AKG College of Engineering, Uttar Pradesh Technical University,NH-24 Bypass, Ghaziabad,UP India; **Nanotechnology Lab, Electrical Engineering Department, MP A&T University, Udaipur, Raj 313001 India; ***Center of Nanobiotechnology, TCC and Florida State University, Tallahassee, FL 32304 USA

ABSTRACT

A search of new class of semiconductors with metal oxides of specific sizes motivated us to synthesize nanoparticles. The preparation of nanocomposites using dispersed nanoparticles into solid hosts is nowadays an attracting scientific art and technological interest. The properties of these hybrid nanocomposite systems are different and often improved, compared with their isolated counterparts. In this study we improved the synthesis of controlled-size semiconductor oxide nanoparticles based on the impregnation and decomposition of transition-metal 2-ethylhexanoate-based precursors in mesoporous hosts aiming to prepare MO2 (M = Ti, Ce, and Sn). The pore size of the host material was enough to control the size of the guest material synthesized within it. The linear mass gain for each cycle in the synthesis process was an advantage of this method, because it allowed the control of nanoparticle growth via a layer-by-layer assembly. We report the results of X-ray diffraction, Compton profiling, transmission electron microscopy, and Raman spectroscopy for SnO2, TiO2 and CeO2 nanocrystals. Raman spectroscopy dependence on nanocrystal sizes allowed nanocrystals to their use by this technique as prompt characterization tool to estimate nanocrystal size.
Keywords: semiconductor, oxide nanoparticles

1 INTRODUCTION

Researches on nanostructured semiconductor materials are the basis for electronics, optoelectronics, sensors, catalysis. Size-induced characteristics give novel properties to aggregate, forming microsized clusters of nanocrystals as integrated chemical system (ICS) as nanoreactors. ICS is heterogeneous and multiphase system (host and guest) designed and arranged (nanocrystals anchored in the pores) for specific functions and/or to carry out specific chemical reactions or processes-photocatalytic activity and photoluminescence intensity of TiO_2 nanoparticles to make high dispersion of Ti ions and/or the coordinative unsaturation of surface Ti ions. Wide band gap semiconductor oxides are SnO_2, TiO_2 and CeO_2 with high photocatalytic activity and high surface to volume ratio. If we consider a spherical particle, the surface to volume ratio exhibits *1/L* dependence, where *L* is the nanoparticle diameter. Nanocrystal synthesis and characterization is focus in this paper.

2. NANOCRYSTAL SYNTHESIS

Metallo-organic decomposition (*MOD*) using layered solids, zeolites, carbon nanotubes. Nanocrystals anchored in porous Vycor glass (PVG, Corning code 7930) with an α-$NbPO_5$ at optimal temperature, atmosphere, time makes inorganic powders and thin films in cycles known as "one impregnation-decomposition cycle – IDC".

3. EXAMPLES OF SYNTHESIS

The integrated chemical systems (nanocrystals anchored on porous hosts) are following as illustration:

3.1. α-$Nbpo_5$ Glass-Ceramic Monolith is obtained from the glass system $6Li_2O–18Nb_2O_5–43CaO–33P_2O_5$ has channel-like pores 130 nm shown in Figure 1a and the SEM image.

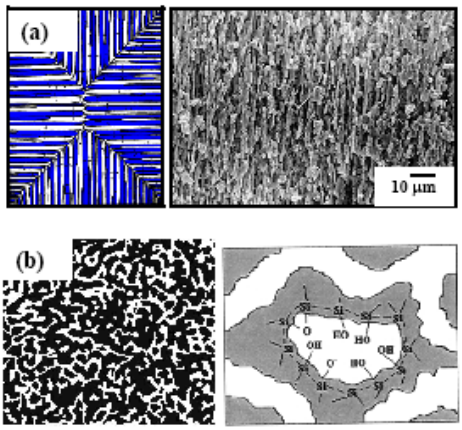

Figure 1. (a) (left) of the popsicle-like structure of porous α-$NbPO_5$ and scanning electron microscope (SEM) image (right) of the host with average pore diameter around 130 nm. (b) The porous structure of PVG (right) and the details of the chemical environmental on the pore surface (left).

3.2. Porous Vycor Glass Monolith (10x10x1) mm^3 with PVG plates in a 2 mol L^{-1} HCl-acetone become rich in silanol (Si–OH) and siloxane (Si–O–Si) groups on surface with pore diameter distribution (2 to 20 nm) .

3.3. Impregnation of Single-Source Precursor into α-$Nbpo_5$ and PVG hosts is done for metallo-organic precursor titanium di-(n-propoxy)-di-(2-ethylhexanoate) [hereafter $Ti(OnPr)_2(hex)_2$ or Ce(III) 2-ethylhexanoate [$Ce(hex)_3$] or Sn(II) 2-ethylhexanoate [$Sn(hex)_2$] impregnated with 50 mL, 1.0 mol L^{-1}, hexane as solvent for 24 h, at room temperature.

3.4. Thermal Decomposition at 600 ^oC for 8 h for $Ce(hex)_3$ at 750 ^oC for 8 h for $Sn(hex)_2$ and $Ti(OnPr)_2(hex)_2$ at ambient atmosphere using a 10 ^oC min^{-1} heating rate removes MO_2@PVG (M = Sn, Ti and Ce) and TiO_2@α-$NbPO_5$ plates at 200 ^0C (impregnation–decomposition cycle or IDC) make free MO_2 (M= Sn, Ti and Ce) nanocrystals.

4. EXAMPLES OF NANOCRYSTALS

4.1.Tin Dioxide is a wide band gap semiconductor with

chemical, optical and electronic properties is useful in catalysis, sensors for fuels and toxic gases, in Li-based batteries. The wide band gap (3.5 eV) makes it optical transparent in the visible region.

4.2. SnO_2 into Porous Hosts shown in Fig. 2a and 2b exhibit a specific diffraction peaks. How size is significant?

The crystallite size, *L*, is given by: $$L = \frac{k \cdot \lambda}{B \cdot \cos\theta} \qquad \textbf{(1)}$$

where k is a geometry dependent constant (about 0.9 for spherical shape), λ is the X-ray wavelength, θ is the Bragg diffraction angle (in rad) and B is full-width at half maximum (FWHM) of the peak after correcting the instrumental broadening which is given by: $$B = \sqrt{B_m^2 - B_s^2} \qquad (2)$$

where B_m and B_s stand for the measured FWHM of the sample and a standard. The SnO_2 crystallite sizes are listed in Table 1 showing pyrolysis of the precursor inside the monoliths makes smaller crystal sizes.

Table 1. Average crystallite sizes estimated by using Scherrer´s model for the semiconductors formed by pyrolysis of the precursors inside and outside (free) host.

	Average crystallite size, *L* (nm)		
Semiconductor	Free	in PVG [3]	in α-$NbPO_5$ [3]
SnO_2	54 [1]	6	14
CdS	24 [2]	5	_ _ _ _ _

Take home points: The linear mass gain is important. Monoliths preserve their porosity and capacity of interacting with single source precursors.

5. Titanium oxide TiO_2 has applications in photocatalysis, optics sensors, with small crystal size and high surface to volume ratio (anatase form). Temperature influences at different heat treatments can be estimated according to the equation: (3)

$$\chi = \frac{1}{1 + 0.8 \cdot \left(\frac{I_A}{I_R}\right)}$$

where χ is the TiO_2^R mass fraction in the powders, while I_A and I_B are the X-ray integrated intensities of the (101) reflection of TiO_2^A and the (110) reflection of TiO_2^R.

5.3. Tio_2@PVG is obtained with 10 IDC (upper trace) is shown in Figure 3a along with the patterns for bulk anatase TiO_2 (lower trace) with average nanocrystal diameter is 5.0 nm. The silicon threshold in the EELS spectra is 103 and 106 eV for Si and SiO_2.

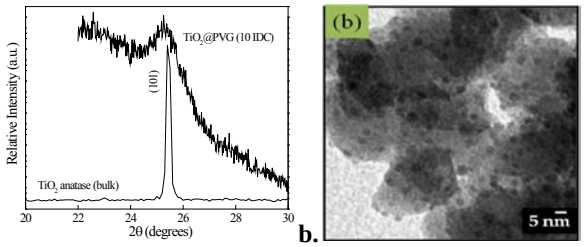

a. **b.**

Figure 2. (a) X-ray powder diffraction patterns for bulk TiO_2 anatase and TiO_2@PVG obtained with 10 IDC. (b) TEM bright field image of TiO_2@PVG obtained with 3 IDC. The average nanocrystal size was found to be 5.0 nm.

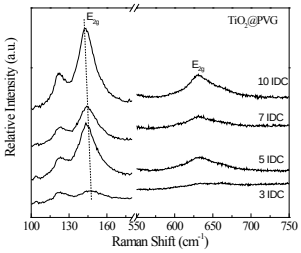

Figure 3. Raman spectra of different TiO_2 nanocrystals size dispersed into PVG obtained from different numbers of IDC.

The Raman spectra characterize by broad bands several peaks from TiO_2 nanocrystals(144 and 635 cm^{-1}, 451 and 615 cm^{-1} of the rutile phase) based on frequency and relative intensity associated with the matrix. The lowest frequency E_{2g} mode experiences an upshift and becomes broader as the number of IDC increases (Figure 3) size-induced phenomena in nanostructured materials. Raman profile is based on the following equation:

$$I(\omega) \alpha \int_{BZ} \frac{|C(0,q)|^2 L^3 q}{[\omega - \omega(q)]^2 + (\gamma/2)^2} \quad (4)$$

where γ is the line width of the Raman peak and ω(q) is the phonon dispersion curve for the bulk counterpart. For spherical nanocrystals $|C(0,q)|^2 = \exp\left(-q^2 L^2 / 16\pi^2\right)$ where *L* is the nanocrystal average diameter. Both γ and *L* are fitting parameters. The phonon confinement is evident for the lowest frequency E_g mode located at ω_0 = 144 cm^{-1} for bulk anatase-TiO_2. For simplicity, phonon dispersion can be of this mode using a linear chain model:

$$\omega(q) = \omega_0 + 20\left[1 - \cos(0.3768q)\right] \qquad (5)$$

As the nanocrystal size gets smaller the phonon confinement involves large q values and the maximum of the Raman peak follows the same trend of ω(q) that is positive in the case of the E_{2g} mode for bulk TiO_2. Figure 4 shows Raman profile of the E_{2g} mode according to Eq. (4) for diameters of 15, 10 and 5 nm and considering Γ_0 = 16 cm^{-1}.

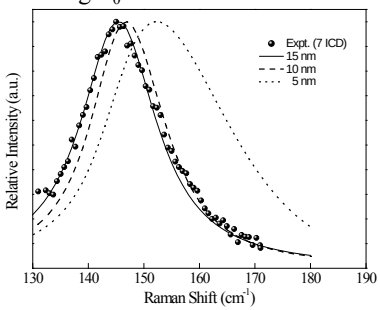

Figure 4. Size dependent Raman scattering profile of the lowest frequency E_{2g} mode for TiO_2. The solid points stand for the experimental data obtained for a TiO_2@PVG sample obtained with 7 IDC. The solid, dashed and dotted lines were obtained by plotting Eq. (4) for nanocrystal diameters of 15, 10 and 5 nm, respectively. The linewidth used was 16 cm^{-1}.[1].

The precursor promotes coverage of the porous surface due to its interaction with the Si–OH sites present in the PVG matrix. The interaction of metallo-organic molecule with Si–OH sites is important and Si–O–Ti bonds in decomposition during nanocrystal formation. The nanocrystal size changes with

transition from anatase to rutile with influence of temperature, nucleation and growth processes at the nanocrystal surface. The anchoring process plays a fundamental role in stabilizing the nanosized-TiO_2 anatase phase.

5.4. Tio2@α-Nbpo5 and role of template: Peaks in XRD pattern of TiO_2^A present a small 2θ variation.. Raman responses of rutile and anatase phases are distinct. TiO_2@α-$NbPO_5$ (A→R) transition Raman spectrum shows bands at 144 cm^{-1} [$E_g(\nu_6)$; vs], 399 cm^{-1} (B_{1g}; m), 519 cm^{-1} (B_{1g}; m) and 639 cm^{-1} [$E_g(\nu_1)$; m] while TiO_2^R exhibits bands at 143 cm^{-1} (B_{1g}; w), 447 cm^{-1} (E_g; s) and 612 cm^{-1} (A_{1g}; s), assigned to phonon lattice modes (where: vs, very strong intensity; s, strong intensity; m, mid-intensity; and w, weak intensity) as shown in Figure 5a. Band at 144 cm^{-1} is intense and no peak of α-$NbPO_5$ host suggests the formation of TiO_2^A phase at 1000 ^oC for 8 h byRaman band at 144 cm^{-1} [Figure 5b]. Role of the template is important in the structural phase of the TiO_2 nanocrystals.

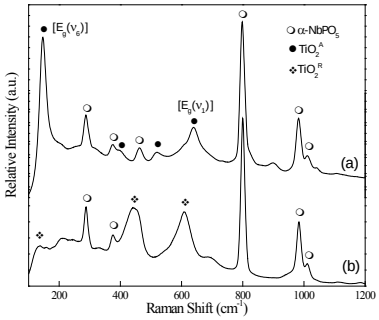

Figure 5. Raman spectra of (a) TiO_2@α-$NbPO_5$and (b) TiO_2@α-$NbPO_5$ with additional thermal treatment at 1000 ^oC for 8 h. [1].

For illustration, Figure 6 shows Raman spectra of TiO_2^A nanocrystals. The [$E_g(\nu_6)$] peak from TiO_2^A changes from 145 cm^{-1} (free) to 148 cm^{-1} (inside the α-$NbPO_5$) and line widths modified from 19 cm^{-1} to 26 cm^{-1} suggest a smaller nanocrystal size *L* when the TiO_2 is prepared inside α-$NbPO_5$ compared with free TiO_2 (600 ^oC for 8 h), which presents *L* = 32 nm for TiO_2^A and *L* = 18 nm for TiO_2^R. The stabilization of TiO_2^A in α-$NbPO_5$ depends on interaction with the surface sites of the pores of α-$NbPO_5$. The smaller the *L*, the larger the fraction of surface sites that are interacting with surface sites of the pores of α-$NbPO_5$, reducing the number of nucleus sites, and causing, as a consequence, an increase in the (A→R) transition temperature. Reduction of *L* leads to increases the growth rate. Example: TiO_2^A@α-$NbPO_5$. In impregnation-decomposition cycles, a total thermal annealing of 80 h at 750 ^oC treatment temperature promote the kinetic coalescence of crystallites. The Raman spectrum of α-$NbPO_5$ exhibits a very strong band at 805 cm^{-1} which is assigned to niobyl groups (Nb=O) from the α-$NbPO_5$ phase; the predominant phase of this porous glass-ceramic [27]. Table 2 shows IDC presents a {$I[\nu(Nb=O)^{805}/I[E_g(\nu_6)^{144}]$ = 1.0} ratio smaller than {$I[\nu(Nb=O)^{805}/I[E_g(\nu_6)^{144}]$ = 1.7} to suggest larger amount of TiO_2^A present in the pores. FWHM of band [$E_g(\nu_6)$] of TiO_2^A in size evaluation depends on growth of *L* and mass increment via impregnation-decomposition cycles. Average TiO_2 nanocrystal inside α-$NbPO_5$ or PVG is different due to the different pore dimensions, i.e., a larger pore diameter allows more solution to get in, increasing the precursor amount, thus leading to larger crystal sizes.

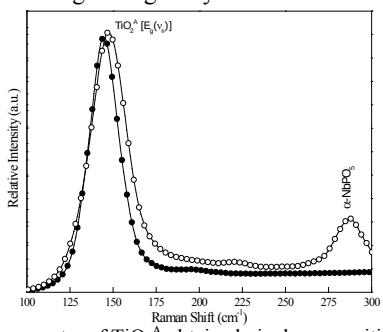

Figure 6. Raman spectra of TiO_2^A obtained via decomposition of (full circle) free $Ti(OnPr)_2(hex)_2$ and (open circle) $Ti(OnPr)_2(hex)_2$@α-$NbPO_5$, in the region between 100-300 cm^{-1} for analysis of band width of the [$E_g(\nu_6)$] phonon lattice mode of TiO_2^A. [1].

Table 2. {$I[\nu(Nb=O)^{805}/I[E_g(\nu_6)^{144}]$} ratio, position and FWHM of Raman bands of the [$E_g(\nu_6)$] phonon lattice mode of the TiO_2^A for: TiO_2^A@α-$NbPO_5$ from 10 IDC, TiO_2^A@α-$NbPO_5$ from 5 IDC and TiO_2^A@α-$NbPO_5$ from 5 IDC+5TT. Reference[1,2]

System	{$I[\nu(Nb=O)^{805}/I[E_g(\nu_6)^{144}]$} ratio	Position (cm^{-1})	FWHM (cm^{-1})
TiO_2@α-$NbPO_5$ from 5 IDC	1.7	147	48
TiO_2@α-$NbPO_5$ from 5 IDC+5TT	1.5	146	40
TiO_2@α-$NbPO_5$ from 10 IDC	1.0	144	26

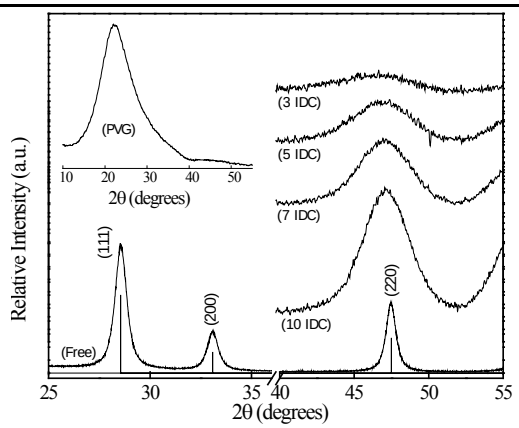

Figure 7. X-ray diffraction patterns for CeO_2@PVG nanocrystals obtained with 3, 5, 7 and 10 IDC. The X-ray pattern at the bottom is for free CeO_2 nanocrystals. The JCPDS standard for bulk CeO_2 is also shown as vertical lines [2]

6.1. Cerium oxide (CeO_2) is used as an active catalyst in vehicle emission systems for oxidation of pollutant gases, as a solid oxide fuel cell electrolyte material, as an electrode material for gas sensors for monitoring environmental pollution, as silicon-on-insulator structures , and as high T_C-superconductors. A route for enhancing the CeO_2 catalyst activity is to increase the surface to volume ratio, which can be achieved with smaller CeO_2 nanoparticles.

6.2. X-ray patterns of Ceo$_2$@PVG CeO_2 nanocrystals dispersed into PVG (obtained with 3, 5, 7, and 10 IDC) showed vertical lines, peak line widths broad suggestive of small size of the nanocrystals. The inset in Figure 7 shows

amorphous state. The shift of the diffraction peak to lower 2θ values indicates a lattice expansion for small CeO_2 particles. These line widths are much broader [≅ 3°] than those expected for bulk crystalline materials, where the diffraction peaks are as narrow as 0.15°. A typical TEM bright field image of the CeO_2@PVG nanocrystals obtained with 7 IDC is shown in Figure 8a. TEM image of the pristine PVG matrix has a different image (Figure 8b).

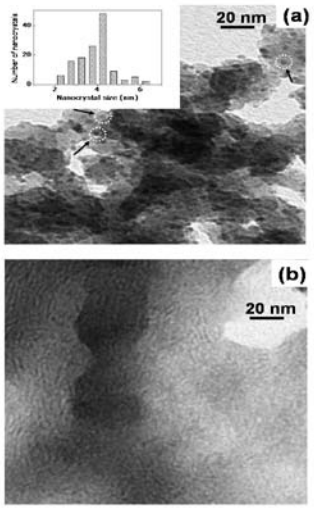

Figure 8. (a) TEM image of CeO_2@PVG nanocrystals obtained with 7 IDC and (b) of PVG. The inset to panel (a) represents particle size distribution. [2].

For illustration, TEM images show average nanocrystal size 2.3, 3.0 and 4.0 nm ± 0.9 nm for 3, 5, and 7 IDC samples similar with X-ray diffraction data. CeO_2 has fluorite structure Fm3m and shows vibrational spectra with one infrared active phonon (T_{1u} symmetry) and one Raman active phonon (T_{2g} symmetry). The T_{2g} Raman mode frequency downshifts and becomes broader as the number of IDC decreases, i.e., as the nanocrystal size decreases shown in Figure 9.

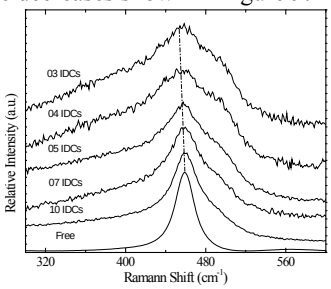

Figure 9. Raman spectra of CeO_2@PVG obtained with 3, 4, 5, 7 and 10 IDC. The Raman spectrum of free (outside the matrix) CeO_2 nanocrystals is also shown. For better comparison, the spectra are normalized to their maximum intensities. [2]

The TEM and Raman spectroscopy indicate strain in Eq. (4). Linear chain model describes the effective phonon dispersion relation and behaviour of the T_{2g} vibrational mode as ω(q) given by: $\omega(q) = 464 - 32[1 - \cos(0.5411q/2)]$ (6)

The phonon dispersion is responsible for involving large *q* wavevectors in the light scattering process. Figure 10a we plot the expected Raman profile of CeO_2 gives nanocrystal diameter as a function of the number of IDC. The nanocrystal average size versus the number of IDC presents a linear behavior. For low diameter nanocrystals the signal-to-noise ratio is poor and the fitting of the Raman profile is difficult.

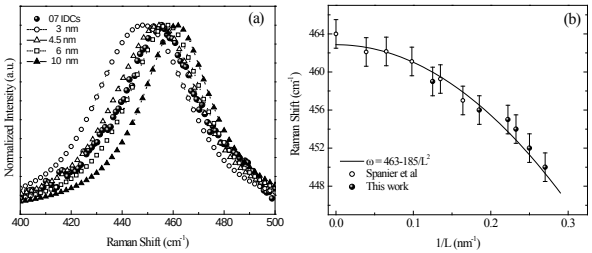

Figure 10. (a) Expected Raman profile for the T_{2g} mode in CeO_2 nanocrystal. (b) Raman frequency as a function of reciprocal nanocrystal size 1/L for CeO_2 nanocrystals.

The changes in lattice parameters and different strain level along the nanoparticle induce small changes in the position of the diffraction peak and broaden the Raman peak. This process leads to non-stoichiometric cerium oxide (CeO_{2-x}) nanocrystals. In the case of Raman scattering, the presence of oxygen vacancies along the nanocrystal also relaxes the q ≅ 0 selection rule which fundamentally has the same effect on the frequency and line width as the nanocrystal size. Raman spectroscopy gives true average diameter size of the nanoparticle distribution. Figure 10b shows the frequency plot of the main Raman peak as a function of the reciprocal nanocrystal size 1/*L*. A fit to the experimental data gives a quadratic dependence of frequency (in units of cm^{-1}) on 1/*L*, i.e.:

$$\omega(L) = 463 - 185/L^2, \qquad (7)$$

where *L* (in units of nm) is the average size of the nanocrystals, considering a spherical shape. CeO_2 nanocrystals can be obtained at 600 °C over 12 h final in size 10 nm. The nanocrystal growth does not occur via coalescence. PVG plays a role in controlling the coalescence process. In the first IDC the precursor promotes coverage of the porous surface, establishing some nucleation sites due to interaction with the Si–OH sites present in the matrix. The metallo-organic molecule is large enough to interact with all nearby Si–OH sites and, during the decomposition process, the dispersed nanocrystals are formed on the nucleation sites and they remain anchored to the porous matrix. The exceeding interfacial free energy is minimized by nanoparticle growth (forbidden coalescence) instead of creating new nucleation sites.

7 CONCLUSION

CeO_2, TiO_2 and SnO_2 nanocrystals have distinct size controllable properties prepared by metallo-organic decomposition, bottom-up approach in nanotechnology. Size-induced Raman spectra peaks of nanocrystals by phonon confinement model supports the average nanocrystal size measurement in TiO_2 and CeO_2 nanocrystals based on size restriction imposed by the pores and anchored through Ti–O–Si linkages. Space restriction and chemical anchoring properties prevent the coalescence process, thus allow control of the nanocrystal size via a linear mass increment.

8 REFERENCES

1. Mazali, I.O et al. Journal of Physics and Chemistry of Solids 66 (2005):37-46.

2. Mazali, I.O et al. Journal of Physics and Chemistry of Solids 68 (2007), 622-627.